NeuroImage 62 (2012) 1342–1353

Contents lists available at SciVerse ScienceDirect

NeuroImage

journal homepage: www.elsevier.com/locate/ynimg

Full Length Articles

Modeling the outcome of structural disconnection on resting-state functional connectivity

Joana Cabral [a,b,*], Etienne Hugues [a], Morten L. Kringelbach [b,c], Gustavo Deco [a,d]

[a] Center of Brain and Cognition, Theoretical and Computational Neuroscience Group, Universitat Pompeu Fabra, Barcelona, Spain
[b] Department of Psychiatry, University of Oxford, Oxford, UK
[c] Center of Functionally Integrative Neuroscience (CFIN), Aarhus University, Denmark
[d] Institut Català de Recerca i Estudis Avançats, Barcelona, Spain

ARTICLE INFO

Article history:
Accepted 3 June 2012
Available online 13 June 2012

Keywords:
Computational model
Structural connectivity
Disconnection
Functional network
Graph-theory
Small-world
Schizophrenia

ABSTRACT

A growing body of experimental evidence suggests that functional connectivity at rest is shaped by the underlying anatomical structure. Furthermore, the organizational properties of resting-state functional networks are thought to serve as the basis for an optimal cognitive integration. A disconnection at the structural level, as occurring in some brain diseases, would then lead to functional and presumably cognitive impairments.

In this work, we propose a computational model to investigate the role of a structural disconnection (encompassing putative local/global and axonal/synaptic mechanisms) on the organizational properties of emergent functional networks. The brain's spontaneous neural activity and the corresponding hemodynamic response were simulated using a large-scale network model, consisting of local neural populations coupled through white matter fibers. For a certain coupling strength, simulations reproduced healthy resting-state functional connectivity with graph properties in the range of the ones reported experimentally. When the structural connectivity is decreased, either globally or locally, the resultant simulated functional connectivity exhibited a network reorganization characterized by an increase in hierarchy, efficiency and robustness, a decrease in small-worldness and clustering and a narrower degree distribution, in the same way as recently reported for schizophrenia patients. Theoretical results indicate that most disconnection-related neuropathologies should induce the same qualitative changes in resting-state brain activity.

Introduction

The spatial patterns observed in brain activity during rest are thought to be shaped by the underlying anatomical structure (Bullmore and Sporns, 2009; Jirsa et al., 2010; Skudlarski et al., 2008). The availability of whole-brain maps of anatomical connections (Hagmann et al., 2008; Kötter, 2004; Sporns et al., 2005) together with computational models of the brain's large-scale neural dynamics have shed light on the relationship between anatomical and functional connectivity (Cabral et al., 2011; Deco et al., 2009; Ghosh et al., 2008; Honey et al., 2007, 2009). Importantly, models can be used to predict the effects of structural alterations on brain dynamics (Alstott et al., 2009; Honey and Sporns, 2008), which is beyond reach on the experimental side, making models a unique tool for the comprehension of brain diseases.

Brain networks have been widely studied by means of graph theory (Bullmore and Sporns, 2009; Rubinov and Sporns, 2010), whether derived from white-matter connections (anatomical networks) or from temporal correlations (functional networks) between brain areas. The application of graph theoretical measures to functional networks derived from blood oxygenation level-dependent (BOLD) signals measured using functional magnetic resonance imaging (fMRI) during rest has shown clinical relevance. Indeed, this procedure has revealed significant alterations in the resting-state patterns of patients with neuropathologies such as schizophrenia (Bassett et al., 2012; Liu et al., 2008; Lynall et al., 2010) and Alzheimer's disease (Supekar et al., 2008), among others.

In this study, we focus on the effects of a structural disconnection on resting-state functional networks. Resting-state functional connectivity is investigated using a model of large-scale ongoing brain neural activity. The model consists of local neural populations dynamically coupled via white-matter anatomical pathways. The coupling weights between neural populations scale the long-distance excitatory strength between brain regions considering simultaneously two factors: 1) the number of white matter fiber tracts detected between those regions using DTI/DSI tractography and 2) the excitatory synaptic weights. From the simulated ongoing brain activity, we estimated the hemodynamic response and computed functional

* Corresponding author at: Universitat Pompeu Fabra, Roc Boronat, 138, 08018 Barcelona, Spain. Fax: +34 93 542 2451.
E-mail address: juanitacabral@hotmail.com (J. Cabral).

1053-8119/$ – see front matter © 2012 Elsevier Inc. All rights reserved.
doi:10.1016/j.neuroimage.2012.06.007

connectivity matrices. Subsequently, simulated functional networks were characterized using graph theory following the methodology from Lynall et al. (2010) for a reliable comparison. In a first step, using a healthy anatomical connectome, we study how the topological organization of simulated functional networks depends on the global structural coupling strength. For a range of coupling strengths, the simulated functional networks were found to have graph properties similar to the ones reported for healthy controls in the work of Lynall et al. (2010). Subsequently, the effects of a pathological disconnection were simulated in two different ways: either by globally decreasing the coupling strength, or by randomly pruning anatomical connections. Theoretical results indicate that, in the model, all disconnections should induce the same qualitative changes.

Schizophrenia is a disorder which has been hypothesized to be related with disconnection effects, and so we have compared our results with experimental measures from schizophrenia patients (Lynall et al., 2010). We found that the reorganization of resting-state functional networks observed between healthy volunteers and people with schizophrenia can be explained by a structural disconnection, both schemes leading to similar results. Overall, these results support the hypothesis that the functional network alterations underlying schizophrenia are caused by a disconnection (encompassing putative local/global axonal/synaptic mechanisms), in agreement with current theories of schizophrenia (Bullmore et al., 1997; Friston and Frith, 1995; Skudlarski et al., 2010; Stephan et al., 2006; Wernicke, 1906; Winterer and Weinberger, 2004; Zalesky et al., 2011). Taken beyond the schizophrenia disorder, our results could provide a new light towards the understanding of altered resting-state functional connectivity occurring in other mental illnesses characterized by disconnection.

Methods

Anatomical connectivity

The brain's anatomical connectivity (AC)—or connectome—is defined as the map of neural connections in the brain. In low-resolution maps such as the ones used here, nodes correspond to segregated brain regions and links are derived from the white matter anatomical pathways interconnecting them. These networks have shown to be a key ingredient to models of resting-state functional connectivity (Cabral et al., 2011; Honey et al., 2009). Given that results can be influenced by the parcellation scheme (Bassett et al., 2011; Zalesky et al., 2010), we used two distinct structural networks (see Fig. 1) in order to be able to generalize: one with $N=90$ brain regions defined using the Automated Anatomical Labelling (AAL) template from Tzourio-Mazoyer et al. (2002), and another with $N=66$ brain regions derived by Hagmann et al. (2008). In both networks, the connectivity strength C_{np} from region p to region n was assumed to be proportional to the number of fibers incoming to region n and inversely proportional to the size of that region (as in Cabral et al. (2011)).

The anatomical brain network with 90 regions was constructed using diffusion tensor imaging (DTI) from the brains of 21 healthy participants following the methodology from Gong et al. (2009). For each subject, a 90×90 weighted network was constructed. Networks were then averaged across subjects resulting in a reliable representation of the anatomical organization of cerebral cortex (see *Supplementary Information (SI)-Methods* for details). For this network, the distance D_{np} between a pair of regions was taken as the Euclidean distance between the corresponding centers of gravity in the AAL template.

The network with 66 regions, previously used in resting-state computational models in Honey et al. (2009) and Cabral et al. (2011), was derived from diffusion spectrum imaging (DSI) by Hagmann et al. (2007) according to the Freesurfer parcellation scheme (surfer.nmr.mgh.harvard.edu (Desikan et al., 2006)) and averaged over 5 healthy subjects. In this case, the distance D_{np} between two regions was given as the average length of the fibers detected connecting these two regions.

The AC in both parcellation schemes, AC_{66} and AC_{90}, is given by the matrices C and D (see Figs. 1B–C).

Simulating disconnection

In the model, local neural networks are connected with each other according to the weight matrix K with $K_{np}=\frac{k}{c_1}C_{np}$. In general, disconnection implies that some or all of these weights decrease, meaning that the disconnected weight matrix K^d has coefficients $K^d_{np}\leq K_{np}$. As there is an infinite number of ways to implement disconnection, we chose two representative examples of it. Note that the specific type of disconnection occurring in a particular disease or in particular patients is out of the scope of the present paper, in which we are interested in the general effects of disconnection on the graph properties of functional networks.

As a first implementation of disconnection, all weights decrease in equal proportion, which is done by decreasing the global coupling strength k ($K^g=(\frac{K_g}{C_1})\ C$, where $k^g<k$). In a second implementation, we have chosen to remove links randomly from the original structural matrix $C_{90\times90}$, a method called random pruning. To simulate the progression of a disconnection disease, we generated a sequence of pruned matrices $C^p_1, \ldots, C^p_m, \ldots, C^p_M$ from the original one, where at each sequence step, a fixed number of links was removed randomly. The corresponding weight matrices write $K^p_m=(\frac{k}{C_1})\ C^p_m$, where the original prefactor k is kept unchanged. Choosing to remove 1% of the total possible links of the binary $C_{90\times90}$ (that is 0.01 $(90)^2=81$ links), which has about 39% of the possible links, a sequence of $M=39$ pruned matrices was generated.

Neural dynamics model

To obtain the BOLD signal during rest, we first simulated the brain's spontaneous neural activity. The model simulates the activity of a network of N brain regions—or nodes—each representing a local network of excitatory and inhibitory neurons. The main assumption of the model is that functional connectivity at the brain-scale level emerges mainly through the interplay between the long-distance brain connectivity and the local node dynamics. For simplicity, the neural networks within a node were assumed to be homogeneous, that is without a specific structure. The nodes are connected via the known AC, given by the $N\times N$ matrices of connection strengths C and inter-regional distances D. We calculate the conduction delay matrix τ dividing the distances by a chosen conduction velocity V ($V=10$ m/s here).

The model is further defined by specifying the dynamics at the node level and how these nodes interact. According to many studies, local neural networks are considered to be in a stable asynchronous state, meaning that neurons tend to fire irregularly and out of synchrony and, in response to a constant input, the network firing rate always decays towards a constant value. Assuming that during rest the mean level of external stimulations remains constant, we hypothesize that the perturbations of neural activity around the constant asynchronous state are small. Therefore, dynamical equations for the evolution of the neural network's firing rate can be written by considering only their linearized version. These equations describe the dynamics of firing rate deviations of local neural networks around their asynchronous state.

To derive the local node dynamical equations, we use a theoretical framework introduced in Mattia and Del Giudice (2002) which describes the dynamics of a neural network. Considering a homogeneous network of neurons, the Fokker–Planck equation (Risken, 1989) describes the temporal evolution of the probability distribution of the neuronal variables over the neural network population. An associated equation gives the neural population firing rate. In this

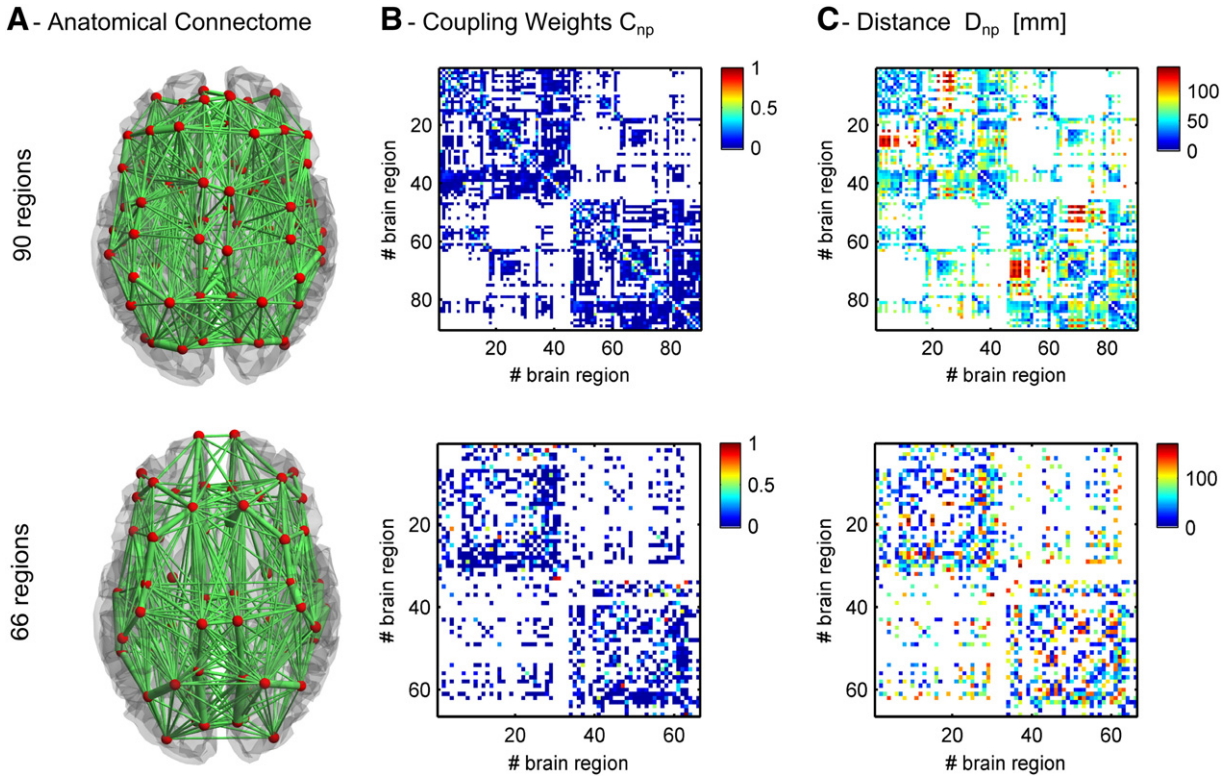

Fig. 1. Large-scale healthy anatomical connectomes used in the model. (Top) Connectome derived from DTI using the AAL template, averaged across 21 healthy subjects. (Bottom) Anatomical connectome derived by Hagmann et al. (2007) using DSI averaged over 5 healthy subjects. (A) Representation of the anatomical connectome. Regions are represented by red spheres placed at their center of gravity. The thickness of the links is proportional to the number of fibers detected in each connection. (B) The weights of the connections are proportional to the number of fibers detected. White color means that no fiber connecting the two corresponding regions was detected. Weights were normalized so that $0<C_{np}<1$. (C) Distance between regions (in mm), given as (top) the Euclidean distance between centers of gravity and (bottom) the average length of the fibers connecting a pair of regions. The list of brain regions and corresponding indexes is reported in SI Tables 1 and 2.

framework, the probability distribution is further decomposed using the infinite series of eigenmodes of the Fokker–Planck equation, giving a nonlinear dynamical equation for each of the coefficients of the series' expansion. Under the hypothesis that the network has a stable asynchronous state, which means a stable steady solution for the Fokker-Planck equation, these equations can be linearized. Then, it can be shown that the dynamics of this infinite set of linear equations is controlled by the infinite set of eigenvalues $\lambda k = -1/\tau_k + i\omega_k$, where $\omega_k/2\pi$ is an oscillation frequency and τ_k a damping timescale. Among these modes, very few have a sufficiently large damping timescale so that they effectively contribute to the dynamics. Usually, one mode has a real eigenvalue, which describes perturbations that simply decay exponentially in time, with a timescale τ_0. As we will use the model results to simulate the BOLD signal, the dynamics produced by the (faster) oscillatory perturbations will be filtered out when calculating the very slow BOLD signal (see Simulated BOLD and functional connectivity). Therefore, we only need to describe the dynamics due to the exponentially decaying perturbations. This dynamics is responsible for the low-frequency part of the neuronal activity. Finally, for the local network n, the firing rate deviations $r_n(t)$ obey the following first order stochastic differential equation:

$$\tau_0 \frac{dr_n}{dt} = -r_n(t) + \frac{k}{c_1}\sum_{p=1}^{N} C_{np} r_p\left(t-\tau_{np}\right) + \sigma\eta_n(t), n = 1,\ldots,N.$$

k is the global excitatory coupling level between nodes ($k>0$). C_{np} and τ_{np} are the structural coupling strength and conduction delay from region p to region n, specified by the Structural Connectivity (SC). Note that the number of fibers, together with the synaptic weights, are accounted for by the coupling strengths. As C has positive coefficients, the Perron–Frobenius theorem shows that this matrix has a real and positive eigenvalue c_1 such that all other eigenvalues are lower in modulus, and therefore have a lower real part. σ is the noise level and the terms $\eta_n(t)$ are uncorrelated white Gaussian noises with zero mean and unit variance ($\langle\eta_n(t)\rangle = 0$ and $\langle\eta_n(t)\eta_p(t')\rangle = \delta_{np}\delta(t-t')$, where δ_{np} is the Kronecker symbol and $\delta(t)$ denotes the Dirac delta function). This noise is not necessarily of external origin (i.e. stimulation noise) and can be generated internally: finite size networks intrinsically induce noise in the dynamics (Mattia and Del Giudice, 2002). As equations are linear, σ only scales the level of the rate deviations. Given τ_0, which is given by the internal state of local networks ($\tau_0 = 20$ ms here), the dynamics depends only on one parameter: k. As long-distance connections are excitatory, the reverberated activity over the network can destabilize the damped local dynamics, and therefore the asynchronous states. For this reason, k must be bounded from above. For null delays, a classical stability analysis gives the stability condition: $k<1$ (explaining why we have scaled down the coupling by c_1 in the previous equation). When delays are finite, this remains a very good approximation.

These equations were numerically integrated using the Euler method with a time-step of 0.1 ms. For every set of parameters considered, we simulated the system for 1200 s (20 min). All calculations were performed using Matlab®.

Without noise, the dynamics of the firing rate deviations around an otherwise constant state would always tend to zero after some time, as long as the stability condition is verified. In the presence of noise, the model permanently produces ongoing fluctuations across the large-scale network by the excitatory reverberation of local activity on this recurrent network. Consequently, even if individual noises are independent, the SC makes the rate fluctuations not independent,

explaining in principle the finding of large-scale structure in the brain fluctuations.

Further, in order to gain theoretical insight into the large-scale network dynamics, it is useful to consider the case of null delays. This case corresponds to the Ornstein–Uhlenbeck process in N dimensions (Gardiner, 2004) but, what makes the dynamics interesting here is the complicated—or disordered—connectivity matrix C, which is the main ingredient in explaining the emergence of specific functional networks as will be shown below. In this case, and using the eigenvectors frame of C, the firing rate deviations can be written as $r(t) = \sum_{p=1}^{N} R_p(t) V_p$ where $r(t)$ and $R(t)$ are the column vectors of the original and transformed rate perturbations, respectively. V_p is the p^{th} unit right eigenvector of the matrix C, associated with the eigenvalue c_p. As the network has a 3 dimensional representation, V_p represents a spatial map (Note that, when considering the case of non-symmetric connectivity matrices, pairs of complex conjugate eigenvalues appear and both conjugate eigenvectors need then to be used to define physically meaningful spatial maps). We sorted these eigenvalues in descending order of the real parts: $c_1 > Re[c_2] > \ldots > Re[c_N]$ ($Re[x]$ denoting the real part of x). Each transformed rate perturbation, or mode, $R_p(t)$ has temporal fluctuations described by the timescale $\tau_p = \tau_0/(1 - kRe[c_p]/c_1)$. From the ordering of the eigenvalues of C, we have $\tau_1 > \tau_2 > \ldots > \tau_N$. Therefore, the global dynamics of the large-scale network is a superposition of these temporal modes, but with distinct spatial maps for each mode. In particular, the modes associated to the eigenvalues with the largest real parts have the largest timescales, and therefore are the slowest ones. Moreover, when the coupling k increases, all modes up to mode p (for which $Re[c_p] > 0 > Re[c_{p+1}]$), get slower and the others get faster. The timescale of the first mode $\tau_1 = \tau_0/(1-k)$ increases faster than all the other timescales τ_p, with $p \geq 2$, and even diverges as $k \to 1$. If we add the fact that the variance of mode $R_p(t)$ is proportional to τ_p, the fluctuations in the network dynamics will be dominated (in variance) by the slowest modes, and dominantly by $R_1(t)$, leading to correlations in the low-frequency part of the neural activity. In particular, the BOLD signal, which can be seen in a first approximation as a low-pass filtering of the neural activity (Cabral et al., 2011), will present spatial correlations. As a result, the mean of the correlation distribution of the BOLD correlation or FC matrix will shift towards positive values.

Because of the finite axonal conduction velocity—in the range of 5 to 10 m/s—delays are in fact finite but generally shorter than 50 ms in humans. Delays theoretically introduce an infinite number of degrees of freedom but their practical effect on the dynamics depends on their magnitude. When the linear dynamical equations are written in the frequency domain, for a given frequency f, delays enter in the terms $\exp(i2\pi f \tau_{np})$. In this study, we are only interested in the BOLD signal generated by the neural activity. Because the model used to calculate the BOLD signal (the Balloon–Windkessel model; see next subsection) first filters the neural activity with a low-pass filter with approximate cut-off at $f_c = 0.4$ Hz (Cabral et al., 2011), and since $f_c \tau_{np} < 0.02$, the delays have a very small effect on the slow part of the neural activity which is responsible for the BOLD signal. Simulations with and without delays confirm, in this particular case, the negligible effect of the delays.

Simulated BOLD signal and functional connectivity

The BOLD signal of each region was estimated from the neural population activity using the Balloon–Windkessel hemodynamic model (Friston et al., 2000, 2003). We focused our investigation on low frequency (0.06–0.125 Hz) fluctuations of the BOLD signal, which have previously been shown to be particularly sensitive to disease-related alterations in schizophrenia (Bassett et al., 2012; Lynall et al., 2010). Simulated BOLD signals were band-pass filtered in that frequency window (0.06 Hz–0.125 Hz) and finally down-sampled at 2 s to have the same temporal resolution as the MR scanner.

Functional connectivity (FC) was evaluated by computing the Pearson correlation of band-passed simulated BOLD signals in different brain areas. This measure is widely employed to derive resting-state functional networks from fMRI signals (Biswal et al., 1995; Fox and Raichle, 2007) and provides a simple characterization of temporal interactions between brain regions. Moreover, comparing with measures from information theory (more precisely the mutual information) which unravels all types of nonlinear interactions, it has recently been shown that correlation captures most of the interaction, and is a very good tool to study the functional connectivity graphs (Hartman et al., 2011; Hlinka et al., 2011). Note that, only to compare the simulated 66×66 FC matrix with the empirical one, the global signal was regressed out (see Fig. 2D and Empirical functional connectivity). The resulting correlation matrix—or FC matrix—can then be studied using graph theory (Achard et al., 2006; Bassett et al., 2012; Lynall et al., 2010; Rubinov and Sporns, 2010).

We analyzed the principal components (PC) of the simulated BOLD signals to obtain a measure of global integration (GI). We computed the covariance matrix and calculated the ratio of the first eigenvalue to the sum of all the others (Friston, 1996; Tononi et al., 1994):

$$GI = \lambda_1 / \sum_{j=2}^{N} \lambda_j$$

From the *Neural Dynamics Model* subsection it can be seen that, as k increases from a sufficiently high value, the first eigenvalue—or variance of the first PC—increases faster than the others, and consequently the GI increases. In fact, mathematically, as the mean of the correlation distribution is positive and increases, the variance of the first PC automatically increases, this PC being the main source of positive correlation.

Empirical functional connectivity

In order to validate the model's performance in reproducing healthy resting-state functional connectivity, we compared simulated functional networks with an empirically derived FC matrix previously used in Honey et al. (2009) and Cabral et al. (2011). This empirical FC matrix was constructed in the parcellation scheme from Hagmann et al. (2007) from the resting brain activity of 5 healthy subjects with eyes closed—the same subjects from which the corresponding SC was obtained. It consists on the correlation matrix of the mean BOLD signal in each of the 66 regions. Before computing the correlation, the BOLD signal was preprocessed for artifact removal including global signal regression (see Honey et al. (2009) for details). Simulated and empirical FC_{66} matrices were compared using Pearson correlation.

Building graphs from functional networks

The set of synthetic functional networks generated with the use of the computational model were characterized using graph theory. To evaluate functional networks by means of graph theory, the FC matrix needs be binarized into an adjacency matrix where correlations above a certain threshold are set to 1 and 0 otherwise. The definition of thresholds depends on either one wishes to create equi-sparse graphs (ensuring a fixed percentage of edges) or equi-threshold graphs (ensuring a minimum correlation value to define an edge, resulting in a variable number of edges) (Bassett et al., 2012). Since the employed graph-theoretical measures are known to depend on the graph's connection density (Bassett et al., 2008, 2012; van Wijk et al., 2010) all our measures refer to equi-sparse graphs defined over a fixed range of connection densities to overcome this dependency. In more detail, from each FC matrix, 14 graphs were constructed with connection densities ranging from 37% to 50% (1% increment) in the same way as in Lynall et al. (2010). Moreover, our networks have 90 and 66 nodes, whereas the experimental results

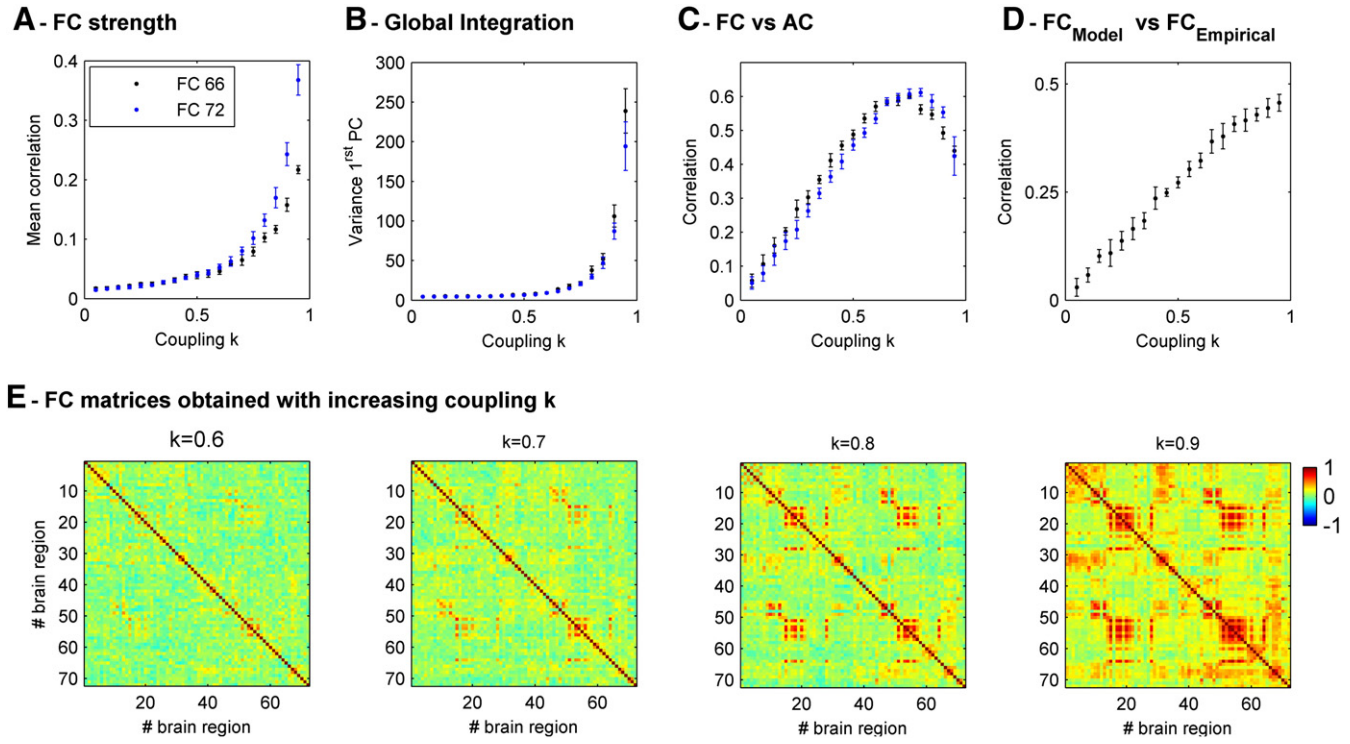

Fig. 2. Dependency of simulated functional connectivity (FC) on the coupling strength *k*. (A) Mean correlation of simulated BOLD signals obtained with increasing coupling strength *k*. (B) Global integration of the BOLD covariance matrix. (C) Correlation between the FC matrix and the underlying anatomical connectivity (AC) matrix. In plots A–C we report the values for the FC matrices with 66 and 72 nodes. (D) Comparison between empirical (healthy) and simulated FC_{66}. The values reported are averaged over 10 runs of 1200 s (error bars = ±1 STD). STD = standard deviation. (E) Example of simulated FC matrices, obtained with increasing coupling strengths *k*.

refer to only 72 nodes—a subgroup of the 90 regions defined in the AAL scheme. To overcome the complex dependency of the measures on the number of nodes (Fornito et al., 2010; van Wijk et al., 2010) and on the parcellation scheme (Wang et al., 2009), we have selected the exact same 72 nodes from the AAL template when analysing the functional networks obtained from simulations with the AC_{90}, resulting in a FC with 72 nodes (FC_{72}). Note that essentially subcortical regions were discarded, but see *SI Table 1* for the list of regions considered. We also report the results using the 66 regions (FC_{66}) to investigate the impact of a different number of nodes in the results.

The various graph measures were estimated for graphs obtained at densities in the range 37–50%, with the exception only for degree distribution parameters, which were only estimated for graphs with 37% density. Measures were averaged across the cost range, providing global measures of the topology of each FC matrix. In addition, the same thresholding technique was applied to 100 random graphs with the same range of connection costs to compare with the simulation results.

Graph theoretical measures

The graph theoretical measures employed were evaluated using the Brain Connectivity Toolbox (Rubinov and Sporns, 2010) and the MatlabBGL Toolbox (Gleich, 2009). For all simulated FC matrices, we first estimated well-known graph measures such as efficiency, clustering and small-worldness. The efficiency is the inverse of the mean shortest path length, i.e. the average number of links (paths) necessary to connect any pair of regions (Latora and Marchiori, 2001). The average clustering indicates the probability of two regions connected to a third one being also connected to each other, forming triangles. Small-worldness depends directly on the two previous measures and evaluates if high efficiency coexists with high clustering, when compared to an equivalent random graph (Humphries et al., 2006; Watts and Strogatz, 1998) (see *SI-Methods* for more details).

We also estimated the hierarchy coefficient β, which is taken as the (positive) exponent of the power-law relationship between the clustering, *Cl*, and the degree, *d*, of the nodes in the network such that $Cl \sim d^{-\beta}$ (Bassett et al., 2008; Ravasz and Barabasi, 2003). β was estimated using the least-squares nonlinear fitting function from Matlab®. The higher the hierarchy coefficient, the more network hubs—defined so for having a large number of connections—have low clustering, meaning that they are more connected to nodes poorly connected to each other.

In addition, we calculated robustness measures, which indicate the graph's resilience to the removal of nodes. When a node is removed either randomly (random attack) or in descending degree (targeted attack), the graph can fragment into independent subgraphs. To estimate the robustness of a graph, each time a node was removed, we recalculated the size of the largest connected component, *s*. Plotting the size $s(n)$ versus the number of nodes removed, *n*, the robustness parameter is defined as the area under this curve (Achard et al., 2006). More robust networks retain a larger connected component even when a large proportion of nodes have been eliminated. To take into account the size of the network, we normalized this value by $N(N-1)/2$, so that the maximum robustness is 1.

Finally, we evaluated the degree distribution of graphs obtained at 37% connection density. This distribution gives the probability of node degrees (Boccaletti et al., 2006), where the node degree is simply defined as the number of edges connecting a node (see Figs. 3J–L). For each simulation, we determined the variance of the degree distribution. In addition, the degree distribution was fitted to a gamma distribution $P(d) \propto d^{\alpha-1} \exp(-d/d_c)$, which was found to be the best fit for experimental results (Lynall et al., 2010). The power exponent, α, and the lower exponential degree cut-off, d_c, were estimated using the least-squares nonlinear fitting function from Matlab®.

Results

Overall, we found that the simulated functional networks generated with the neurodynamical model specified in Neural Dynamics Model

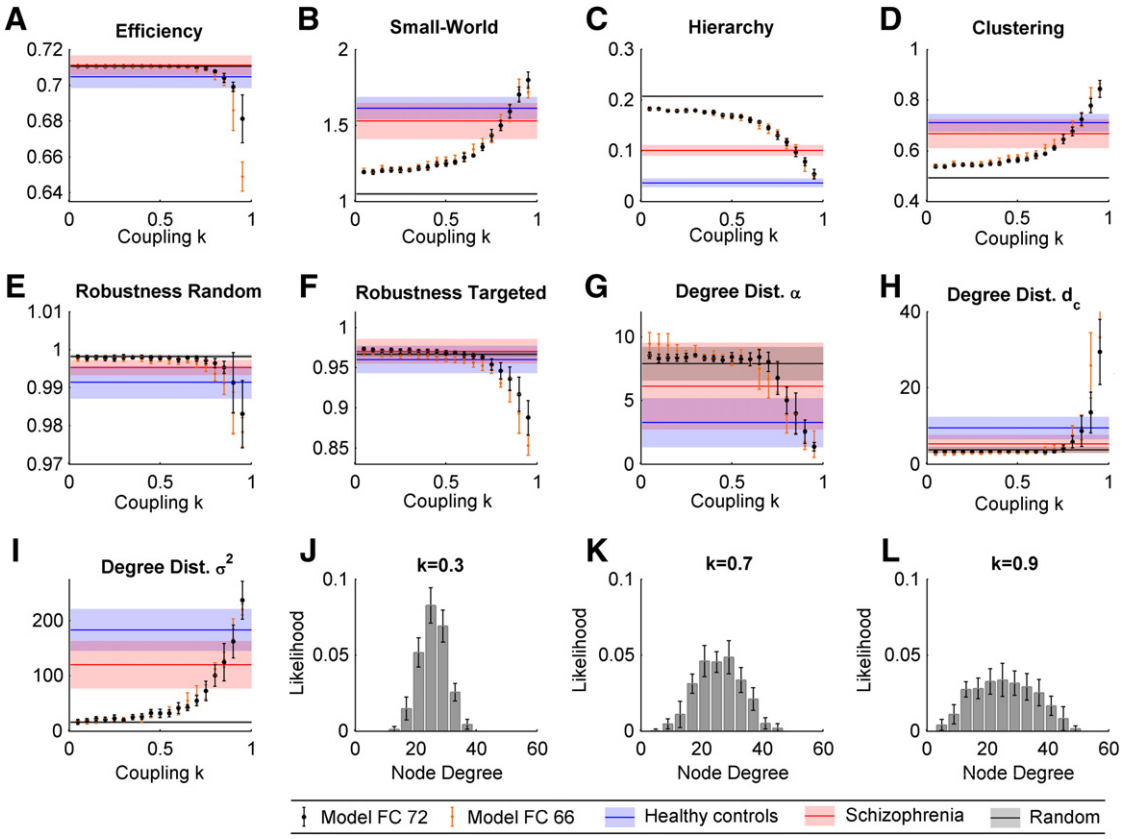

Fig. 3. Dependency of simulated functional networks on the structural coupling strength and comparison with empirical results reported in health and schizophrenia. (A–I) Simulated functional networks obtained with the model with increasing structural coupling strength k are characterized using graph theory. Black error-bars (mean ± 1 STD) correspond to results from simulated FCs considering the same 72 brain regions used in Lynall et al. (2010), whereas orange error-bars correspond to results using another anatomical parcellation (66 regions). For comparison we indicate the values for healthy controls (blue) and schizophrenia patients (red) reported in Lynall et al. (2010). Shaded bands indicate the confidence interval of 1 STD. In addition, measures of equivalent random networks are reported (grey), showing that, as the coupling is decreased (from right to left), simulated functional networks become randomized. (J–L) Example of degree distributions obtained with increasing coupling k. Error bars indicate the confidence interval of 1STD across 10 simulation runs. (For interpretation of the references to color in this figure legend, the reader is referred to the web version of this article.)

depend largely on the underlying structural connectivity. First, using a healthy AC we studied how parameters such as correlation strength, global integration and a number of measures from graph theory, vary as a function of the global coupling strength k. This coupling strength, encompassing axonal and synaptic mechanisms, uniformly scales all the connection weights between brain regions defined by the neuroanatomical network (see Anatomical connectivity). Then, we considered two particular disconnection schemes: one by decreasing the global coupling strength, the other by randomly removing links from the anatomical network while the absolute coupling strength remained fixed. Furthermore, we theoretically generalized the previous results to any disconnection scheme. Finally, we analyzed our results in light of the schizophrenia literature, mainly focusing on a recent study from Lynall et al. (2010) who reported altered resting-state functional networks in people with schizophrenia in terms of graph theory.

Simulated functional connectivity

Using our model of ongoing brain neural activity, we studied how the anatomical connectivity leads to the functional connectivity, and particularly how this depends on the global coupling. For low couplings ($k \leq 0.5$) the simulated BOLD signals are weakly correlated (Fig. 2A) because there is no dominant mode in the neural activity, as seen by the global integration measure (Fig. 2B). As the coupling strength increases above these values, and due to the progressive emergence of a dominant mode, positive correlations build up and the FC matrix becomes increasingly shaped by the underlying SC (Fig. 2C). Above a sufficient coupling, more and more regions that are not structurally connected become also correlated: the correlation with the empirical FC keeps increasing (Fig. 2*D*) while the correlation between AC and FC decreases (Fig. 2*C*). However, in the proximity of the critical coupling the dynamics becomes too globally integrated ($\lim_{k_c \to 1}(GI) = \infty$) (see Fig. 2 *B*). Remarkably, both FC_{66} and FC_{72} depend similarly on the coupling strength (in *SI* Fig. 2 we show that these properties are maintained even when considering the simulated dataset with 90 regions, FC_{90}). The variance in results (errorbars) is due to the effect of the dynamical noise in the model and to the finite duration of the simulated time series (1200 s here).

Graph properties of simulated functional connectivity

We analyzed simulated functional networks using a number of measures from graph theory. As shown in Fig. 3, the different measures employed appear to vary with the coupling strength in a continuous fashion. When the coupling value is too small ($k \leq 0.5$), the simulated FC graphs share properties of random graphs (reported in grey in Figs. 3*A-I*). In this region the small-world index is close to 1 (Fig. 3B), the average clustering coefficient is low (Fig. 3*D*) and the degree distribution is narrow (Fig. 3I) and bell-shaped (Figs. 3G–*H*,*J*) with a low probability of both low- and high-degree nodes, typical of a random graph. As a consequence of having less high-degree hubs, random graphs are more robust to attacks, because these can maintain connectedness even after the removal of a large number of nodes (Figs. 3*EF*). On the other hand, a higher hierarchy in random graphs indicates that nodes with higher clustering are the ones with lesser degree (Fig. 3*C*). As the coupling increases from 0.5 to 0.95 the functional networks reorganize and most

of the metrics evolve towards values characteristic of healthy human FC (reported in blue) (Lynall et al., 2010). Namely the clustering coefficient and the small-world index increase, the hierarchy decreases and the degree distribution becomes wider (Figs. 3I, L). In addition, functional networks become less robust to attacks, especially the targeted ones (Figs. 3E–F). Remarkably, we find that healthy human FC graph properties can be approximately obtained when the coupling is in the range $0.85<k<0.9$.

Effects of global and local disconnection

For the first type of disconnection considered, the coupling was uniformly reduced and all graph properties were found to change monotonically (Fig. 3). In order to simulate other types of disconnection, which are more localized, we pruned the original structural connectivity matrix, building a sequence of pruned matrices by successively removing 1% of the possible links in a random fashion (see Simulating disconnection). The absolute global coupling level (k/c_1) is otherwise kept constant. We started from the healthy case using a fixed coupling value of 0.87, with which we obtained approximate healthy human FC graph properties. As illustrated in Figs. 4AC, we found that successive pruning induces monotonical changes in the graph properties of emergent FCs, in the same way as decreasing the global coupling.

Calculating the leading eigenvalue $c^p_{m,1}$ of the pruned matrices (see Fig. 4*B*), we found that it decreases as pruning progresses. Therefore, keeping the absolute global coupling level k constant is equivalent to taking a global coupling $k^p_m = kc^p_{m,1}/c_1$, which decreases as pruning evolves (see *SI-Text* for a theoretical demonstration and *SI* Figs. 3 and 4). In other words, pruning the matrix is equivalent to decreasing the global coupling, and consequently, the graph properties change in the same direction as for the previous disconnection scheme.

More generally, as we theoretically demonstrate in *SI-Text*, for any conceivable disconnection the leading (positive) eigenvalue of a connectivity matrix decreases (at least when this matrix is symmetric). This generalization includes even the case of removed nodes (as done by Alstott et al. (2009) to simulate lesions), where removing a node is equivalent in the model to remove all connections to that node (see *SI-Text*). Here, we found numerically the same behaviour for non-symmetric connectivity matrices. In conclusion, according to the present model, any disconnection leads to the same type of topological reorganization of resting-state functional graphs.

Importantly, we found that when the AC is only partially pruned (up to 15% of removed links), it is possible to recover the graph properties of healthy functional networks by increasing the global coupling strength (see *SI* Fig. 3). Only when the underlying AC is further disconnected, then the few remaining links are not sufficient to shape the resulting FC with graph properties characteristic of humans, and remain random even at high global coupling.

Simulated functional networks in schizophrenia

In this section, we concentrated on the specific case of disrupted functional networks in schizophrenia during rest. In the work from Lynall et al. (2010) the graph measures explored herein were found to expose significant differences between functional networks from healthy controls and patients with schizophrenia. Notably, they found that functional networks from people with schizophrenia were more efficient, less small-world, more hierarchical, less clustered, more robust, and with more homogeneous regional degrees (i.e. narrower degree distribution) than healthy functional networks.

In the present work, disrupted functional networks in schizophrenia are hypothesized to be related to a widespread decrease in the long-range excitatory strength between brain regions, i.e. the coupling parameter k in the model. This decreased coupling could be caused by a pathological disconnection, in agreement with current pathophysiological theories of schizophrenia (Stephan et al., 2006). On one side, the

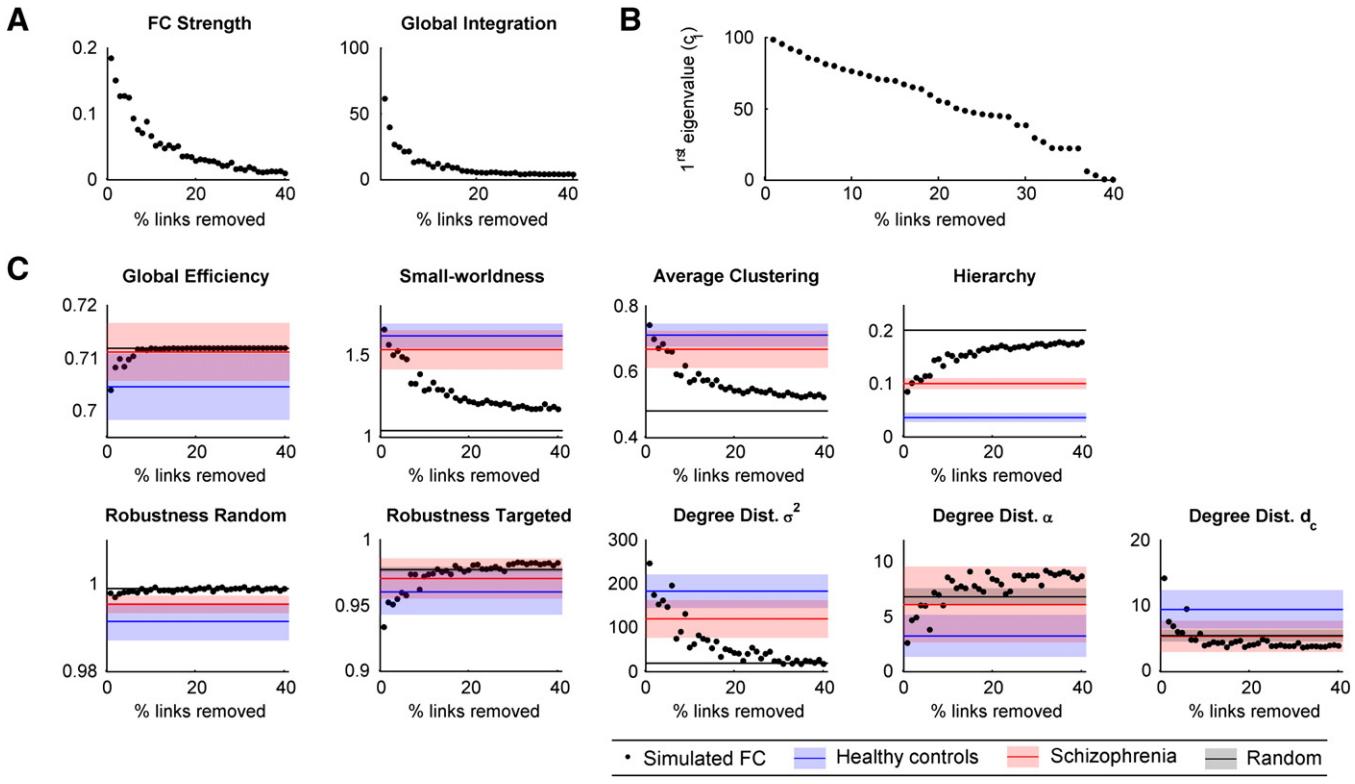

Fig. 4. Effects of pruning links in the anatomical connectivity (AC) on the properties of emergent functional connectivity (FC) obtained with fixed coupling ($k=0.87$). (A) The mean correlation and the global integration of BOLD signals decrease as links are removed from the anatomical network AC_{90}. (B) As links are removed, the first eigenvalue of the pruned matrices decreases. (C) Graph theoretical properties of simulated functional connectivity obtained with increasingly pruned AC matrices. Pruning consisted on successively removing 1% of the possible links in a random fashion.

disconnection could be due to a decrease in white matter connectivity (Wernicke, 1906), supported by a number of studies reporting lower fractional anisotropy (Lim et al., 1999; Mitelman et al., 2006; Skudlarski et al., 2010), less axonal fibers interconnecting gray-matter regions (Zalesky et al., 2011) and myelin-related dysfunction (Davis et al., 2003) in patients with schizophrenia. Even so, the hypothesis of anatomical disconnection in schizophrenia still needs further validation (see for example van den Heuvel et al. (2010)). Alternatively, the decoupling in the model could still be interpreted as related to a damage occurring at the synaptic level, associated to a deficient modulation of synaptic plasticity (Friston, 1998; Stephan et al., 2006) and/or possibly related to reports of dopaminergic (Winterer, 2006; Winterer and Weinberger, 2004), cholinergic (Mobascher et al., 2011; Winterer, 2010), or glutamatergic (Coyle et al., 2003) malfunction in schizophrenia. Importantly, the mechanisms leading to a decreased coupling strength are not necessarily exclusive and could coexist (Stephan et al., 2006).

In order to compare our graph theoretical results in a statistical way with the ones from Lynall et al. (2010), we started by defining two groups of coupling strengths (with 30 values each), one representative of healthy controls, K_H, and another of patients with schizophrenia, K_S. We have chosen to define these values based on the global integration of BOLD signals (see Simulated BOLD signal and functional connectivity) which was found in Lynall et al. (2010) to be significantly reduced in people with schizophrenia ($GI_S = 32.6 \pm 11\%$) compared to healthy volunteers ($GI_H = 43.1 \pm 8.4\%$). Based on these measures, we defined a set of 30 values taken from a Gaussian distribution $g(GI_H)$ with mean = 43.1 and 8.4% standard deviation and 30 values taken from another distribution $g(GI_S)$ with mean = 32.6% and 11% standard deviation (see Fig. 4A for an illustration). Then, we extrapolated the coupling strengths necessary in the model to match each of the expected *GI* values. In this way, we obtained two groups of coupling strengths with 30 values each ($K_H = 0.85 \pm 0.01$STD and $K_S = 0.81 \pm 0.02$STD), statistically representative of the healthy controls and the patients with schizophrenia in terms of global integration of BOLD signals. Subsequently we ran simulations using these coupling values and analyzed the resulting functional networks using graph theory.

In a first step, we analyzed the sensitivity to fragmentation of functional graphs obtained at K_H and K_S. Bassett et al. (2012) found that equi-threshold graphs built from resting-state functional networks from healthy controls lose connectedness at lower costs than the ones from schizophrenia patients. To evaluate if the same phenomenon occurs in our simulated networks we calculated the size of the largest connected component as a function of the graph density, with densities ranging from 0% to 100% (with 1% increment). We did it using the complete simulated set of 90 regions (same as used in Bassett et al. (2012)) Remarkably, the same type of tendency was observed in simulated functional graphs (see Fig. 5B left). Moreover, above 27% cost, all simulated graphs exhibited full connectedness, so at the costs used for graph theory (37–50%) all graphs are fully connected. In addition, we also estimated the sensitivity to fragmentation using equi-threshold graphs, where functional connections were considered as a link only when the correlation was above a certain threshold, ranging from 0 to 1 (0.01 increment) (see Fig. 5B right). In this case, functional graphs from schizophrenia patients fragment at lower thresholds. This illustrates the fact that fragmentation, as well as other graph measures, depend largely on the thresholding technique. For the following analysis, we show the results using exactly the same thresholding method from Lynall et al. (2010) for a reliable comparison,

The graph metrics obtained for each population (K_H and K_S) are shown in Fig. 5C (black +) in comparison with the equivalent experimental results (blue and red error bars). Notably, all the changes in the metrics followed the same tendency as reported experimentally. Namely, as can be observed in Fig. 5C the functional graphs obtained at lower coupling (K_S) were more efficient, less clustered, more hierarchical, less small-world and more robust to both random and targeted attack than the functional graphs obtained with around 5% higher coupling (K_H). In addition, in the group with lower coupling the degree distributions had a smaller variance and fitted to gamma distributions with higher power exponent and smaller degree cut-off (Figs. 5C–D). Functional graphs obtained at higher couplings, on the contrary, exhibit a degree distribution with a larger variance which reflects in higher probability of both high and low degree nodes, as observed also by a less steep cumulative degree distribution (Fig. 5E). Finally, the percentage of variance accounted for by the first PC was significantly reduced at lower couplings, as expected, but no significant difference was found in the remaining PCs (Fig. 5F). Although most of the metrics were found to be in the same range as the ones reported experimentally (error bars in Fig. 5C), some of the metrics, such as the robustness to targeted attack and the hierarchy in the healthy population, were consistently different from experiments.

These results show a tight relationship between the global integration of BOLD signals and graph theoretical properties of functional networks. Moreover, they corroborate our hypothesis that the functional network alterations observed in schizophrenia could result from a decrease in the coupling strength between cortical regions, which scales the global integration of BOLD signals and consequently the properties of emergent functional networks. Please note that a homogeneous reduction in the coupling strength affects functional connectivity in a heterogeneous fashion. Again, we remind that this pathological disconnection could originate either from disruption of axonal connectivity or by malfunction at the synaptic level, unifying current theories of schizophrenia.

Discussion

In the present work, we used a modeling approach to investigate the role of structural connectivity in shaping functional networks as measured with fMRI during rest. Structural connectivity is ensured by brain mechanisms involved in long-range signal transmission in the brain, including axonal connectivity (dependent on the number, density and coherence of axon fibers) and synaptic mechanisms (e.g. neurotransmission and plasticity). As shown here, a disruption of these mechanisms, at either a global or a local level (such as occurring in certain brain pathologies), can have dramatic impacts on the resulting functional networks.

Large-scale neural models of brain dynamics are promising tools to explore the non-trivial relationship between anatomical and functional brain connectivity. In particular, these models allow for an investigation of the role of different factors (here, the long-range excitation) in the BOLD signal dynamics, the resulting functional networks and their topological properties. Furthermore, investigating the impact of such factors in the AC-FC relationship helps understanding the mechanisms underlying healthy resting-state activity and its breakdown in disease. In general, our results show that resting-state functional networks depend largely on the structural coupling strength.

First, the results from our model show that stronger structural coupling generates more globally correlated and globally integrated BOLD signals. This is due to the increased excitatory reverberation across the large-scale network, which increases the timescale and the relative variance of the slowest dynamical mode, faster than for the other modes. Using a healthy anatomical connectome, we found an optimal structural coupling strength for which the simulated functional networks have graph-theoretical properties very similar to those of resting-state functional networks in healthy brains. Namely, simulated functional graphs exhibit small-world properties, characterized by high clustering and relatively high efficiency, low hierarchical organization, and a high probability of both high- and low-degree nodes, as indicated by the degree distribution parameters. The robustness to attacks is decreased with more hub regions. As the coupling is reduced, emergent functional graphs become successively more random and, in the case of an extreme

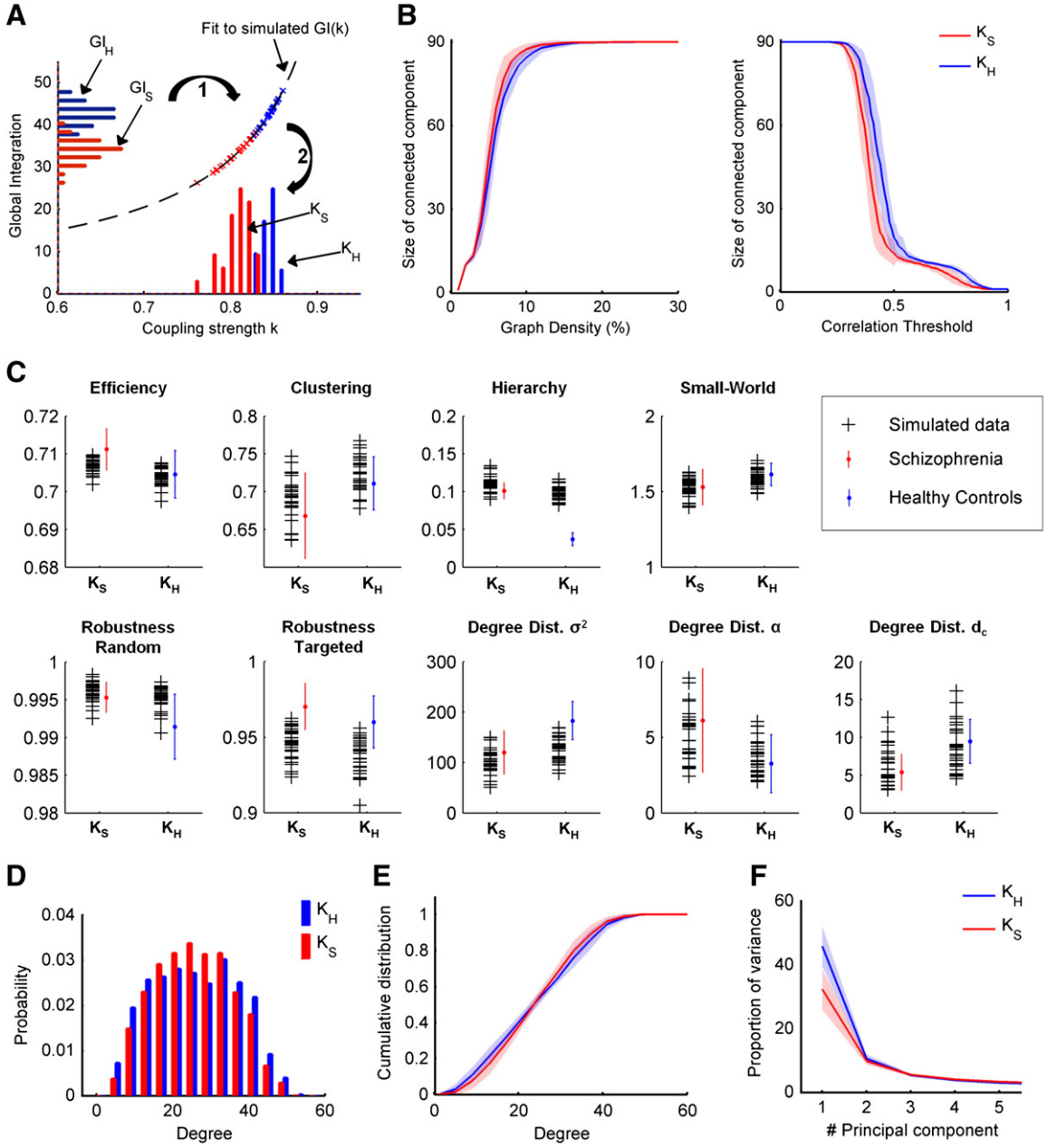

Fig. 5. Properties of simulated functional networks in health and schizophrenia. (A) Definition of coupling values K_H and K_S representative of the healthy controls and the schizophrenia patients, based on the global integration values reported experimentally for the two groups, GI_H and GI_S. Using a fitting function, we searched which coupling values would give the same GI distributions, resulting in two distributions of couplings K_H (0.85 ± 0.01STD) and K_S (0.81 ± 0.02STD). (B) Fragmentation of simulated functional networks. Networks simulated with K_S were found to be more connected at lower densities when comparing equi-sparse graphs (left). However, comparing equi-threshold graphs, they fragmented at lower thresholds than networks obtained with K_H. (C). Graph theoretical metrics of simulated FC matrices (black +) together with experimental values in health (blue: mean ± std) and schizophrenia (red mean ± std) reported in Lynall et al. (2010). (D–E) Pooled degree probability density (D) and cumulative degree distribution (E) for the two populations obtained with K_H (blue) and K_S (red). (F) Percentage of variance accounted for by the first 10 principal components of the simulated BOLD signal. (For interpretation of the references to color in this figure legend, the reader is referred to the web version of this article.)

disruption of the structural coupling (i.e. > 50% of coupling decrease) the simulated functional networks share properties of random networks.

Disconnection effects were studied by considering a uniform decrease in the structural connectivity strength. Nevertheless, pathological disconnections may happen only between specific brain regions and therefore affect distinct functional systems depending on the location of the disruption. To take into account the effects of local disconnections in our study, we have also considered pair-wise disconnections occurring in a random and non-uniform way. As links are randomly removed from the anatomical connectome and the absolute coupling is kept constant, we find that the simulated functional networks reorganize in the same way as if the (relative) structural coupling was decreased. We provide a theoretical demonstration to explain why this is actually the case. For symmetric connectivity, we found that any type of disconnection, including the case where nodes are eliminated from the network, will decrease the leading positive eigenvalue of the matrix and therefore the absolute coupling appears lower, generalizing our results for such type of connectivity. Moreover, we found that, when the AC is only partially pruned, it is possible to recover the graph properties of healthy functional networks by increasing the global coupling strength. Only when the underlying AC is further disconnected, then it is no more possible to obtain FC graph properties characteristic of humans, even at high coupling levels.

Disrupted functional networks in schizophrenia

Schizophrenia is generally thought to be linked to a pathological disconnection, supported by mounting evidence of disrupted inter-regional functional interactions (measured with fMRI). However, the pathophysiological origin of this disconnection remains under debate. Possible explanations rely mainly on the neural structures involved in signal transmission, i.e. axons and synapses. Importantly, in our model the coupling parameter encompasses both mechanisms and therefore can be interpreted in the light of both theories of schizophrenia.

Results show that disrupted structural connectivity—or disconnection—occurring at either a global or a local level, is indeed a strong candidate to explain the alterations reported in functional brain networks of people with schizophrenia during rest. Importantly, very good quantitative agreement with the functional network reorganization observed in schizophrenia was found with a uniform decrease of only 5% in the coupling or a removal of about the same proportion of existing links (both types of measures being equivalent in terms of fiber changes). This was characterized by a decrease in small-worldness and clustering and an increase in hierarchy, efficiency, robustness and degree homogeneity.

Existing experimental studies (Bassett et al., 2012; Lynall et al., 2010) have shown that the BOLD signals from schizophrenia patients are significantly less globally integrated than the ones from healthy controls. Based on these results, we defined a range of coupling values that originate, through the model, simulated BOLD signals with statistically similar values of global integration found in disease and healthy states. We found that less globally integrated simulated BOLD signals give rise to simulated functional networks with properties matching the ones characteristic of the schizophrenia disease.

Our results propose a general scenario for understanding elements of schizophrenia, unifying structural (e.g. axonal and/or synaptic mechanisms), dynamical (e.g. BOLD signal integration) and functional connectivity studies (e.g. graph properties of functional networks).

Relationship between structural coupling strength and cognitive performance

The role of the topological organization of functional networks on the performance of cognitive integration has long been speculated (Sporns et al., 2004). For example, a small-world topology of functional networks is thought to support both modular and distributed processing dynamics (Bassett and Bullmore, 2006; Sporns et al., 2002), leading to optimal information processing in the brain. In addition, Lynall et al. (2010) found a strong link between a number of graph theoretical measures of functional networks and a verbal fluency score (indicative of cognitive performance).

Here we propose that the functional network (dis) organization leading to cognitive impairment can be directly linked to a disruption of the underlying structural connectivity (potentially axonal or synaptic). This hypothesis is corroborated by a number of studies that have reported a link between structural connectivity and behavioural/emotional symptoms in schizophrenia (Hoptman et al., 2004; Skelly et al., 2008; Skudlarski et al., 2010; Stephan et al., 2009). With the present model, we show a direct relationship between graph measures of functional networks (previously related to cognitive performance) and the underlying structural connectivity. These results reinforce the idea that a stronger structural coupling between cortical regions allows a better integration of the functional networks, hypothetically leading to an increased cognitive performance. Note that a widespread decrease in the structural coupling between brain regions results in a heterogeneous decrease in inter-regional regional functional connectivity. Therefore the relationship suggested by these results between lower structural coupling and decreased cognitive performance should be seen as independent from functional connectivity strength. Indeed, the relationship between functional connectivity strength and cognitive performance is likely to be more complex. A recent study from Hawellek et al. (2011) has found that inter-regional functional connectivity within the default mode network increased (rather than decreased) with the decline of cognitive performance in multiple sclerosis. However since the global signal was regressed out in the preprocessing of BOLD signals—which greatly complicates the interpretation of BOLD signal correlations (Murphy et al., 2009), it is premature to draw conclusions based on this result.

Relation to other modeling studies

Over the last few years, several large-scale models of the brain activity have studied how the resting FC could be derived from the AC using a neural mass model at the local node level. Following several reduction lines, local node models have included a conductance-based biophysical model (Alstott et al., 2009; Honey et al., 2007, 2009), the FitzHugh–Nagumo model (Ghosh et al., 2008), the Wilson-Cowan model (Deco et al., 2009) and a phase oscillator like in the Kuramoto model (Cabral et al., 2011). Independently, here we propose a new derivation based on the framework of the Fokker-Planck equation, which is able to describe the full network dynamics, taking into account the effect of noise. Under the hypothesis that the local dynamics is asynchronous, a hypothesis with significant experimental support, we derived a simplified linear model based on the supplementary hypothesis that deviations from this dynamical state are small. At the end, we have not only a rigorous derivation of the model, but also the advantage that the linearity of the model allows for a theoretical understanding of the behavior of the large-scale model and of the resulting FC. Such an understanding is much more difficult in the other nonlinear models. Moreover, although there is a qualitative difference between models, the performance of our model in predicting the empirical FC is very similar to the one from existing models, indicating no clear advantage of taking into account nonlinear effects to predict the resting FC.

Other modeling studies have studied the impact of lesions in functional connectivity during rest (Alstott et al., 2009; Honey and Sporns, 2008). Although lesions were simulated by removing nodes or cortical areas in the brain, it can be seen as a particular type of disconnection, where all links to a certain node (or area) are removed. One of the main findings was that FC alterations can be widespread even when the lesion is local. Moreover, FC changes were found to be very dependent on the brain regions affected by the lesion (Alstott et al., 2009). Although a study of the spatial alterations in FC is beyond the scope of the present study, the present model sheds a new light on these previous results.

In our model, the slowest modes are responsible for the low-frequency correlations, in particular the slowest one. When we consider the case of a global disconnection, we do not change the connectivity matrix, and in that case, the smooth FC changes are mainly due to the change in relative variance of the first (slowest) mode, which reflects spatially in its spatial map. When we consider a local disconnection (or a lesion), the connectivity matrix changes and the spatial maps also change: therefore, FC changes non-locally, crucially and non-trivially depending on the lesion site, in the same way eigenvectors depend non-trivially on the underlying matrix.

Limitations and further studies

Although computational models serve to test existing theories and to make predictions, results must be interpreted in light of the model limitations.

First, we used averaged anatomical connectomes. Although averaging helps eliminating spurious connections detected by the tracking algorithm and therefore provide a robust and reliable version of the human connectome, the variability across subjects in those terms is neglected. In Fig. 4 we define variability across subjects by means of the structural coupling k, which is proposed to be one (but not the only) source of variability across subjects. Furthermore, the anatomical

connectomes refer to healthy participants and disconnection effects were modeled by inducing uniform or heterogeneous alterations in the SC. We believe our model results would benefit if simulations were ran using anatomical connectomes from people with disconnection-related pathologies. Due to the increasing availability of anatomical connectomes in health and disease (e.g. from the Human Connectome Project www.humanconnectomeproject.org) such studies should be implemented in the future. In addition, the use of low-resolution parcellation templates (e.g. 66 and 90 regions) limits our model to reproduce only large-scale patterns of BOLD activity. Using connectomes with higher spatial resolution would allow a more comprehensive study regarding smaller substructures of the brain's network. Even so, in general terms, the characteristics of functional networks explored herein were found to vary with the structural coupling in a consistent way, with disregard to the parcellation schemes used (90 and 66 regions). Note that the graph measures reported by Lynall et al. (2010) and reproduced in this work can only be qualitatively compared because functional networks were derived in a similar way and the same thresholding technique was applied. For example, in a recent study from Yu et al. (2011) functional networks derived using independent component analysis exhibited higher (rather than lower) clustering coefficients and path lengths in schizophrenia. Therefore, we find it necessary to establish standardized methods for analyzing brain networks by means of graph theory, to allow a direct comparison of these measures across studies. In addition, it should be noted that the randomization effects observed not only in the model but also in experiments depend largely on the thresholding technique. In fact, to avoid comparing graphs with different densities, fixed cost values were established to build graphs, which forces then lower correlation thresholds and subsequently a decrease in correlation significance.

Beyond the decrease of BOLD FC in schizophrenia, Rubinov et al. (2009) have reported an increase of FC using EEG. However, since the present model only considers low frequency neural activity for the computation of the BOLD FC, this apparent contradiction cannot be investigated in this study.

Finally, it is important to have in mind that experimental results are also subject to methodological limitations due to limited sample sizes and artifacts introduced by the imaging techniques. For example, the mean FC strength reported in the experiments (Lynall et al., 2010) was consistently higher than in simulations. This correlation shift to higher positive values could be induced by some remaining global artefacts in the BOLD signal (like those due to heartbeat and respiration) since no pre-processing step was intended to eliminate them.

Appendix A. Supplementary data

Supplementary materials related to this article can be found online at http://dx.doi.org/10.1016/j.neuroimage.2012.06.007.

References

Achard, S., Salvador, R., Whitcher, B., Suckling, J., Bullmore, E., 2006. A resilient, low-frequency, small-world human brain functional network with highly connected association cortical hubs. J. Neurosci. 26, 63–72.

Alstott, J., Breakspear, M., Hagmann, P., Cammoun, L., Sporns, O., 2009. Modeling the impact of lesions in the human brain. PLoS Comput. Biol. 5, e1000408.

Bassett, D.S., Bullmore, E., 2006. Small-world brain networks. Neuroscientist 12, 512–523.

Bassett, D.S., Bullmore, E., Verchinski, B.A., Mattay, V.S., Weinberger, D.R., Meyer-Lindenberg, A., 2008. Hierarchical organization of human cortical networks in health and schizophrenia. J. Neurosci. 28, 9239–9248.

Bassett, D.S., Brown, J.A., Deshpande, V., Carlson, J.M., Grafton, S.T., 2011. Conserved and variable architecture of human white matter connectivity. Neuroimage 54, 1262–1279.

Bassett, D.S., Nelson, B.G., Mueller, B.A., Camchong, J., Lim, K.O., 2012. Altered resting state complexity in schizophrenia. Neuroimage 59, 2196–2207.

Biswal, B., Yetkin, F.Z., Haughton, V.M., Hyde, J.S., 1995. Functional connectivity in the motor cortex of resting human brain using echo-planar MRI. Magn. Reson. Med. 34, 537–541.

Boccaletti, S., Latora, V., Moreno, Y., Chavez, M., Hwang, D.-U., 2006. Complex networks: structure and dynamics. Phys. Rep. 424, 175–308.

Bullmore, E., Sporns, O., 2009. Complex brain networks: graph theoretical analysis of structural and functional systems. Nat. Rev. Neurosci. 10, 186–198.

Bullmore, E.T., Frangou, S., Murray, R.M., 1997. The dysplastic net hypothesis: an integration of developmental and dysconnectivity theories of schizophrenia. Schizophr. Res. 28, 143–156.

Cabral, J., Hugues, E., Sporns, O., Deco, G., 2011. Role of local network oscillations in resting-state functional connectivity. Neuroimage 57, 130–139.

Coyle, J.T., Tsai, G., Goff, D., 2003. Converging evidence of NMDA receptor hypofunction in the pathophysiology of schizophrenia. Ann. N. Y. Acad. Sci. 1003, 318–327.

Davis, K.L., Stewart, D.G., Friedman, J.I., Buchsbaum, M., Harvey, P.D., Hof, P.R., Buxbaum, J., Haroutunian, V., 2003. White matter changes in schizophrenia: evidence for myelin-related dysfunction. Arch. Gen. Psychiatry 60, 443–456.

Deco, G., Jirsa, V., McIntosh, A.R., Sporns, O., Kotter, R., 2009. Key role of coupling, delay, and noise in resting brain fluctuations. Proc. Natl. Acad. Sci. U.S.A. 106, 10302–10307.

Desikan, R.S., Segonne, F., Fischl, B., Quinn, B.T., Dickerson, B.C., Blacker, D., Buckner, R.L., Dale, A.M., Maguire, R.P., Hyman, B.T., Albert, M.S., Killiany, R.J., 2006. An automated labeling system for subdividing the human cerebral cortex on MRI scans into gyral based regions of interest. Neuroimage 31, 968–980.

Fornito, A., Zalesky, A., Bullmore, E.T., 2010. Network scaling effects in graph analytic studies of human resting-state FMRI data. Front. Syst. Neurosci. 4, 22.

Fox, M.D., Raichle, M.E., 2007. Spontaneous fluctuations in brain activity observed with functional magnetic resonance imaging. Nat. Rev. Neurosci. 8, 700–711.

Friston, K.J., 1996. Theoretical neurobiology and schizophrenia. Br. Med. Bull. 52, 644–655.

Friston, K.J., 1998. The disconnection hypothesis. Schizophr. Res. 30, 115–125.

Friston, K.J., Frith, C.D., 1995. Schizophrenia: a disconnection syndrome? Clin. Neurosci. 3, 89–97.

Friston, K.J., Mechelli, A., Turner, R., Price, C.J., 2000. Nonlinear responses in fMRI: the Balloon model, Volterra kernels, and other hemodynamics. Neuroimage 12, 466–477.

Friston, K.J., Harrison, L., Penny, W., 2003. Dynamic causal modelling. Neuroimage 19, 1273–1302.

Gardiner, C.W., 2004. Handbook of stochastic methods for physics, chemistry and the natural sciences. Springer-Verlag.

Ghosh, A., Rho, Y., McIntosh, A.R., Kotter, R., Jirsa, V.K., 2008. Cortical network dynamics with time delays reveals functional connectivity in the resting brain. Cogn. Neurodynamics 2, 115–120.

Gleich, D.F., 2009. Models and Algorithms for PageRank Sensitivity, Stanford University, url= http://www.stanford.edu/group/SOL/dissertations/pagerank-sensitivity-thesis-online.pdf.

Gong, G., Rosa-Neto, P., Carbonell, F., Chen, Z.J., He, Y., Evans, A.C., 2009. Age- and gender-related differences in the cortical anatomical network. J. Neurosci. 29, 15684–15693.

Hagmann, P., Kurant, M., Gigandet, X., Thiran, P., Wedeen, V.J., Meuli, R., Thiran, J.P., 2007. Mapping human whole-brain structural networks with diffusion MRI. PLoS One 2, e597.

Hagmann, P., Cammoun, L., Gigandet, X., Meuli, R., Honey, C.J., Wedeen, V.J., Sporns, O., 2008. Mapping the structural core of human cerebral cortex. PLoS Biol. 6, e159.

Hartman, D., Hlinka, J., Palus, M., Mantini, D., Corbetta, M., 2011. The role of nonlinearity in computing graph-theoretical properties of resting-state functional magnetic resonance imaging brain networks. Chaos 21, 013119.

Hawellek, D.J., Hipp, J.F., Lewis, C.M., Corbetta, M., Engel, A.K., 2011. Increased functional connectivity indicates the severity of cognitive impairment in multiple sclerosis. Proc. Natl. Acad. Sci. U.S.A. 108, 19066–19071.

Hlinka, J., Palus, M., Vejmelka, M., Mantini, D., Corbetta, M., 2011. Functional connectivity in resting-state fMRI: is linear correlation sufficient? Neuroimage 54, 2218–2225.

Honey, C.J., Sporns, O., 2008. Dynamical consequences of lesions in cortical networks. Hum. Brain Mapp. 29, 802–809.

Honey, C.J., Kotter, R., Breakspear, M., Sporns, O., 2007. Network structure of cerebral cortex shapes functional connectivity on multiple time scales. Proc. Natl. Acad. Sci. U.S.A. 104, 10240–10245.

Honey, C.J., Sporns, O., Cammoun, L., Gigandet, X., Thiran, J.P., Meuli, R., Hagmann, P., 2009. Predicting human resting-state functional connectivity from structural connectivity. Proc. Natl. Acad. Sci. U.S.A. 106, 2035–2040.

Hoptman, M.J., Ardekani, B.A., Butler, P.D., Nierenberg, J., Javitt, D.C., Lim, K.O., 2004. DTI and impulsivity in schizophrenia: a first voxelwise correlational analysis. Neuroreport 15, 2467–2470.

Humphries, M.D., Gurney, K., Prescott, T.J., 2006. The brainstem reticular formation is a small-world, not scale-free, network. Proc. R. Soc. Biol. Sci. 273, 503–511.

Jirsa, V.K., Sporns, O., Breakspear, M., Deco, G., McIntosh, A.R., 2010. Towards the virtual brain: network modeling of the intact and the damaged brain. Arch. Ital. Biol. 148, 189–205.

Kötter, R., 2004. Online retrieval, processing, and visualization of primate connectivity data from the CoCoMac database. Neuroinformatics 2, 127–144.

Latora, V., Marchiori, M., 2001. Efficient behavior of small-world networks. Phys. Rev. Lett. 87, 198701.

Lim, K.O., Hedehus, M., Moseley, M., de Crespigny, A., Sullivan, E.V., Pfefferbaum, A., 1999. Compromised white matter tract integrity in schizophrenia inferred from diffusion tensor imaging. Arch. Gen. Psychiatry 56, 367–374.

Liu, Y., Liang, M., Zhou, Y., He, Y., Hao, Y., Song, M., Yu, C., Liu, H., Liu, Z., Jiang, T., 2008. Disrupted small-world networks in schizophrenia. Brain 131, 945–961.

Lynall, M.E., Bassett, D.S., Kerwin, R., McKenna, P.J., Kitzbichler, M., Muller, U., Bullmore, E., 2010. Functional connectivity and brain networks in schizophrenia. J. Neurosci. 30, 9477–9487.

Mattia, M., Del Giudice, P., 2002. Population dynamics of interacting spiking neurons. Phys. Rev. E Stat. Nonlin. Soft Matter Phys. 66, 051917.

Mitelman, S.A., Newmark, R.E., Torosjan, Y., Chu, K.W., Brickman, A.M., Haznedar, M.M., Hazlett, E.A., Tang, C.Y., Shihabuddin, L., Buchsbaum, M.S., 2006. White matter fractional anisotropy and outcome in schizophrenia. Schizophr. Res. 87, 138–159.

Mobascher, A., Warbrick, T., Brinkmeyer, J., Musso, F., Stoecker, T., Shah, N.J., Vossel, S., Winterer, G., 2011. Nicotine effects on attention in schizophrenia: a simultaneous EEG-fMRI study. Eur. Neuropsychopharmacol. 21, S515–S516.
Murphy, K., Birn, R.M., Handwerker, D.A., Jones, T.B., Bandettini, P.A., 2009. The impact of global signal regression on resting state correlations: are anti-correlated networks introduced? Neuroimage 44, 893–905.
Ravasz, E., Barabasi, A.L., 2003. Hierarchical organization in complex networks. Phys. Rev. E Stat. Nonlin. Soft Matter Phys. 67, 026112.
Risken, H., 1989. The Fokker–Planck Equation: Methods of Solutions and Applications. Springer Series in Synergetics. Springer.
Rubinov, M., Sporns, O., 2010. Complex network measures of brain connectivity: uses and interpretations. Neuroimage 52, 1059–1069.
Rubinov, M., Knock, S.A., Stam, C.J., Micheloyannis, S., Harris, A.W., Williams, L.M., Breakspear, M., 2009. Small-world properties of nonlinear brain activity in schizophrenia. Hum. Brain Mapp. 30, 403–416.
Skelly, L.R., Calhoun, V., Meda, S.A., Kim, J., Mathalon, D.H., Pearlson, G.D., 2008. Diffusion tensor imaging in schizophrenia: relationship to symptoms. Schizophr. Res. 98, 157–162.
Skudlarski, P., Jagannathan, K., Calhoun, V.D., Hampson, M., Skudlarska, B.A., Pearlson, G., 2008. Measuring brain connectivity: diffusion tensor imaging validates resting state temporal correlations. Neuroimage 43, 554–561.
Skudlarski, P., Jagannathan, K., Anderson, K., Stevens, M.C., Calhoun, V.D., Skudlarska, B.A., Pearlson, G., 2010. Brain connectivity is not only lower but different in schizophrenia: a combined anatomical and functional approach. Biol. Psychiatry 68, 61–69.
Sporns, O., Tononi, G., Edelman, G.M., 2002. Theoretical neuroanatomy and the connectivity of the cerebral cortex. Behav. Brain Res. 135, 69–74.
Sporns, O., Chialvo, D.R., Kaiser, M., Hilgetag, C.C., 2004. Organization, development and function of complex brain networks. Trends Cogn. Sci. 8, 418–425.
Sporns, O., Tononi, G., Kotter, R., 2005. The human connectome: a structural description of the human brain. PLoS Comput. Biol. 1, e42.
Stephan, K.E., Baldeweg, T., Friston, K.J., 2006. Synaptic plasticity and dysconnection in schizophrenia. Biol. Psychiatry 59, 929–939.
Stephan, K.E., Friston, K.J., Frith, C.D., 2009. Dysconnection in schizophrenia: from abnormal synaptic plasticity to failures of self-monitoring. Schizophr. Bull. 35, 509–527.
Supekar, K., Menon, V., Rubin, D., Musen, M., Greicius, M.D., 2008. Network analysis of intrinsic functional brain connectivity in Alzheimer's disease. PLoS Comput. Biol. 4, e1000100.
Tononi, G., Sporns, O., Edelman, G.M., 1994. A measure for brain complexity: relating functional segregation and integration in the nervous system. Proc. Natl. Acad. Sci. U.S.A. 91, 5033–5037.
Tzourio-Mazoyer, N., Landeau, B., Papathanassiou, D., Crivello, F., Etard, O., Delcroix, N., Mazoyer, B., Joliot, M., 2002. Automated anatomical labeling of activations in SPM using a macroscopic anatomical parcellation of the MNI MRI single-subject brain. Neuroimage 15, 273–289.
van den Heuvel, M.P., Mandl, R.C., Stam, C.J., Kahn, R.S., Hulshoff Pol, H.E., 2010. Aberrant frontal and temporal complex network structure in schizophrenia: a graph theoretical analysis. J. Neurosci. 30, 15915–15926.
van Wijk, B.C., Stam, C.J., Daffertshofer, A., 2010. Comparing brain networks of different size and connectivity density using graph theory. PLoS One 5, e13701.
Wang, J., Wang, L., Zang, Y., Yang, H., Tang, H., Gong, Q., Chen, Z., Zhu, C., He, Y., 2009. Parcellation-dependent small-world brain functional networks: a resting-state fMRI study. Hum. Brain Mapp. 30, 1511–1523.
Watts, D.J., Strogatz, S.H., 1998. Collective dynamics of 'small-world' networks. Nature 393, 440–442.
Wernicke, C., 1906. Grundrisse der Psychiatrie. Thieme, Leipzig, Germany.
Winterer, G., 2006. Cortical microcircuits in schizophrenia—the dopamine hypothesis revisited. Pharmacopsychiatry 39, S68–S71.
Winterer, G., 2010. Why do patients with schizophrenia smoke? Curr. Opin. Psychiatry 23, 112–119.
Winterer, G., Weinberger, D.R., 2004. Genes, dopamine and cortical signal-to-noise ratio in schizophrenia. Trends Neurosci. 27, 683–690.
Yu, Q., Sui, J., Rachakonda, S., He, H., Gruner, W., Pearlson, G., Kiehl, K.A., Calhoun, V.D., 2011. Altered topological properties of functional network connectivity in schizophrenia during resting state: a small-world brain network study. PLoS One 6, e25423.
Zalesky, A., Fornito, A., Harding, I.H., Cocchi, L., Yucel, M., Pantelis, C., Bullmore, E.T., 2010. Whole-brain anatomical networks: does the choice of nodes matter? Neuroimage 50, 970–983.
Zalesky, A., Fornito, A., Seal, M.L., Cocchi, L., Westin, C.F., Bullmore, E.T., Egan, G.F., Pantelis, C., 2011. Disrupted axonal fiber connectivity in schizophrenia. Biol. Psychiatry 69, 80–89.